ÖAW ÖSTERREICHISCHE AKADEMIE DER WISSENSCHAFTEN

HEPHY INSTITUTE OF HIGH ENERGY PHYSICS

Superconducting thermometers for the direct detection of light dark matter

Felix Wagner

Institute of High Energy Physics of the Austrian Academy of Sciences

Quantum technologies lecture series, CERN, June 2023

Dark matter

cosmic microwave background (CMB)

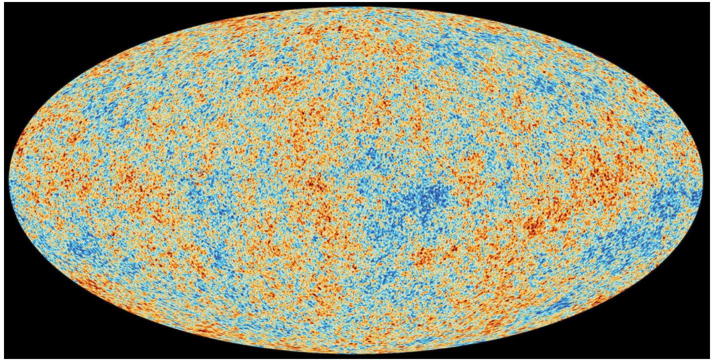

© ESA and the Planck Collaboration

bullet cluster (1E 0657-56)

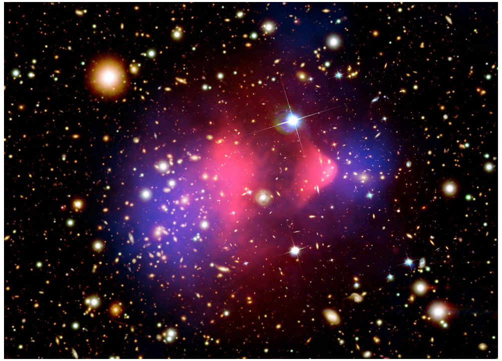

© X-ray: NASA/CXC/CfA/M.Markevitch, Optical and lensing map: NASA/STScI, Magellan/U.Arizona/D.Clowe, Lensing map: ESO WFI

galactic rotation curve (Messier M33)

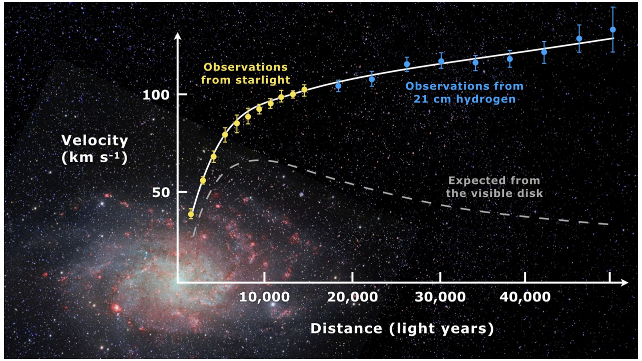

© CC BY-SA 4.0, source: wikimedia

We observe overwhelming gravitational evidence for the existence of non-luminous, stable, cold, non-baryonic "dark" matter (DM) in our universe.

Best estimate from CMB: **(83.9 +- 1.5)%* of all matter in our universe is DM.**

Many particle candidates: (generalized) WIMPs, Axions, SIMPs, …

The mass scale of a hypothetical DM particle is not fixed.

*A&A 641, A6 (2020)

Direct detection

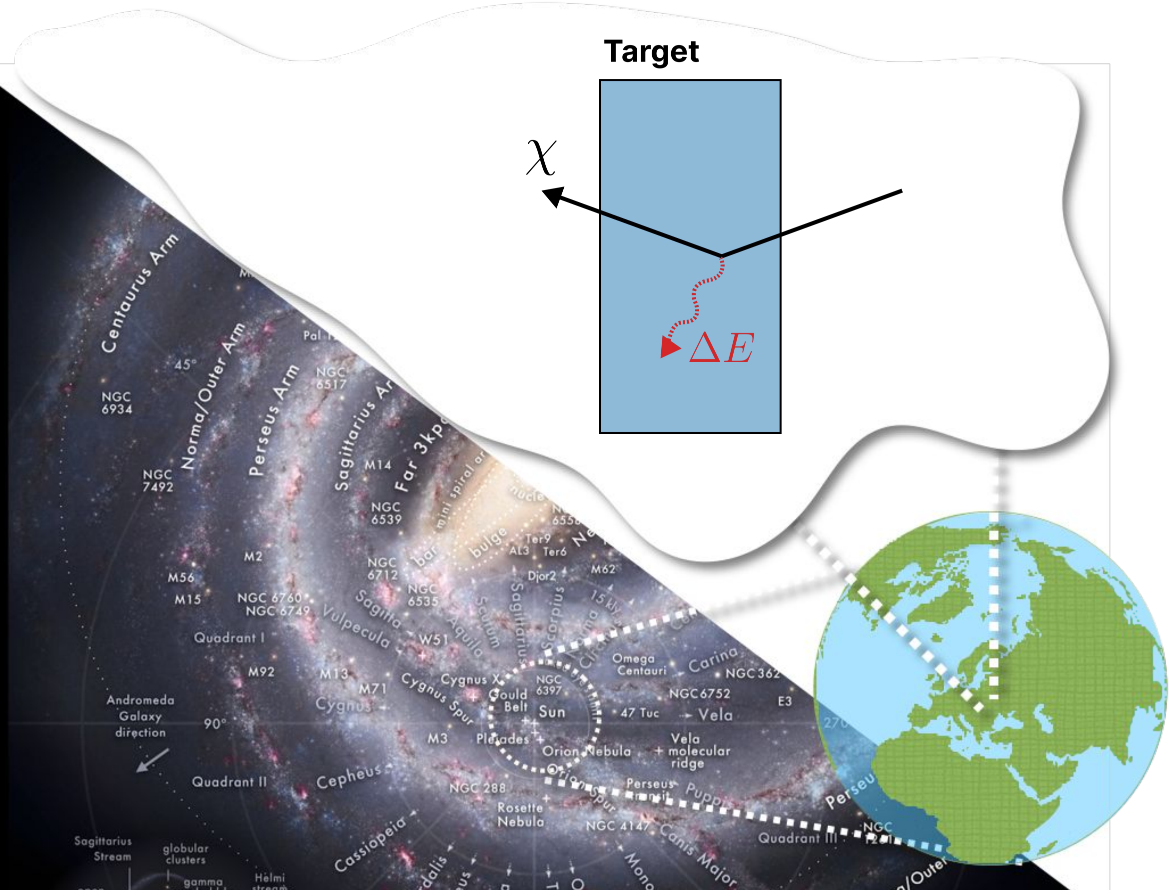

DM velocity distribution in Milky Way can be approximated with Maxwellian distribution.

Density along the solar circle is **~0.4 GeV/c^2/cm^3***.

Direct detection experiments test DM models via DM-target scattering.

Likelihoods depend on assumed DM mass and interaction cross section σ with target.

*Nature Phys 11, 245–248 (2015)

Expected scattering rate

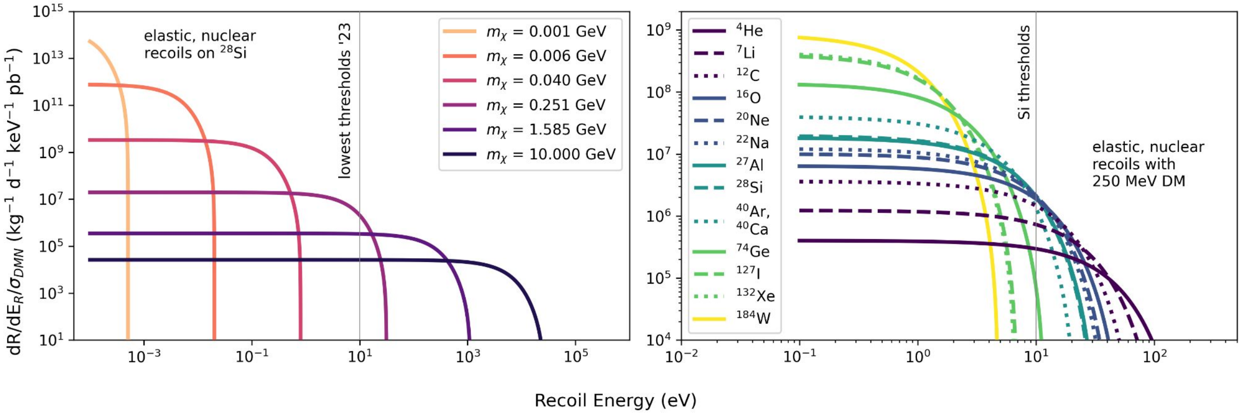

Massive DM particles scatter elastically and spin-independently off target nuclei.

Objectives of (ideal) direct DM search: low energy threshold, high target mass.

Light DM and heavy nuclei reduce expected recoil energy ⇒ experiments use

- high target mass and heavy nuclei for heavy DM searches,
- **low threshold and light nuclei for light DM searches.**

spectra calculated following
Phys. Rev. D 31, 3059 (1985)
astrophysical parameters from
Rev. Mod. Phys. 85, 1561 (2013)
Phys. Rev. D 92, 083517 (2015)
A&A 523, A83 (2010)
Monthly Notices of the Royal Astronomical Society 379, 755 (2007)
Monthly Notices of the Royal Astronomical Society 221, 1023 (1986)

Exclusion limits on DM-nucleus elastic scattering

Cryogenic calorimeters with superconducting thermometers reach the best energy thresholds and sensitivity for sub-GeV/c^2 DM.

For higher DM masses time projection chambers (TPCs) with liquid noble gases are most sensitive.

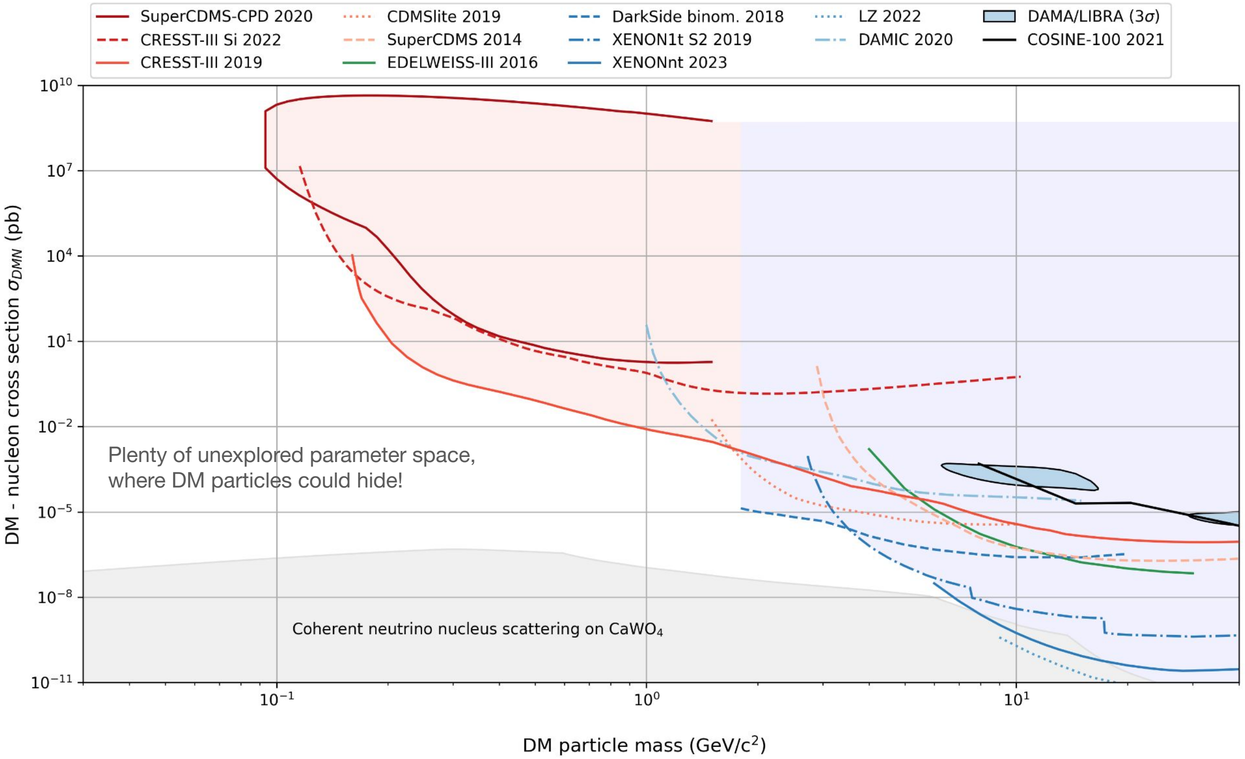

Detection channels

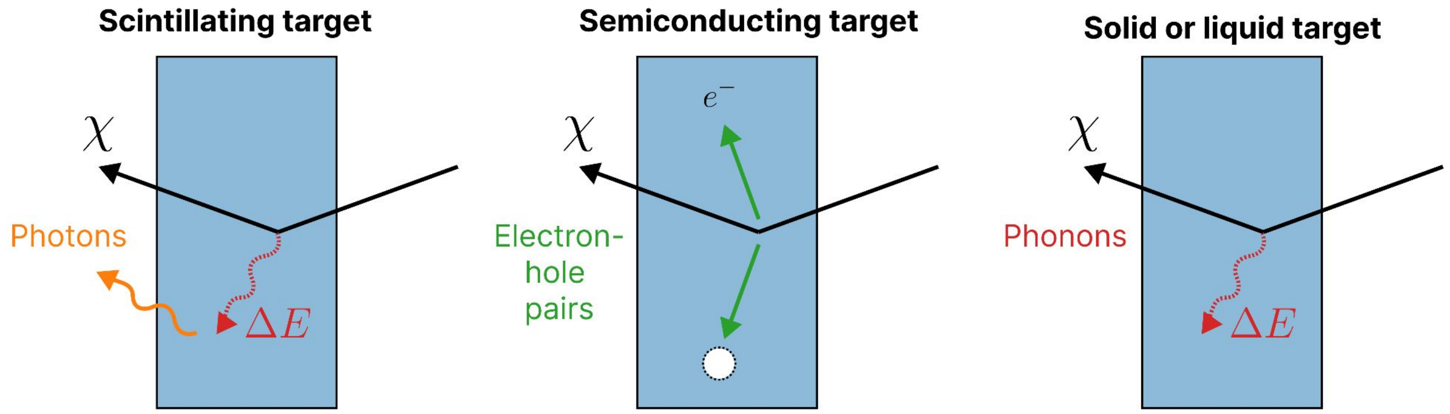

Signal channels to detect target scattering:

- scintillation (photons) measurable with scintillating crystals, liquids or gases,
- ionisation (electron-hole pairs) measurable with semiconductors, certain liquids, gases,
- **lattice vibrations (phonons) measurable (mostly) with single crystals**.

Measured recoil energy depends on scattering particle

Particle-independent energy scale!

Often multiple signal channels used for event discrimination, e.g. scintillating crystals.

Superconducting thermometers

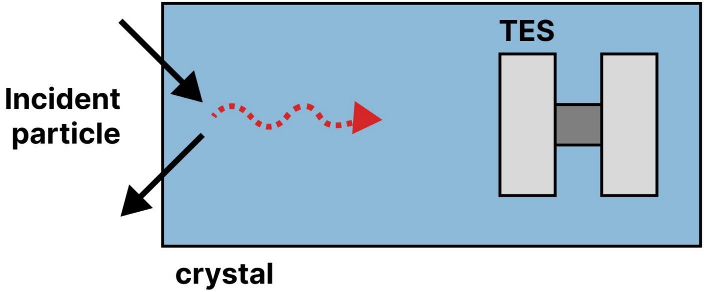

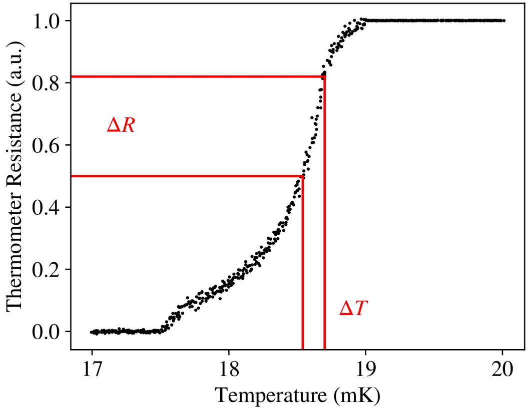

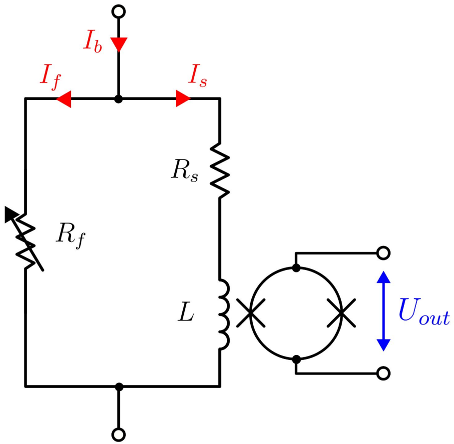

Transition edge sensor (TES): superconducting film operated in the transition from its normal to superconducting state. Operation in low-noise SQUID-based readout circuit turns temperature/resistance fluctuations into measurable quantities.

⇒ **thermometer sensitive to ≈ uK**.

Film is thermally coupled to target crystal, collecting phonons from particle recoils in target.

⇒ **recoils down to 10 eV recoil energy detectable**.**

Technology developed in mid 90's* and continuously improved for DM searches by experiments (**CRESST, CDMS**, et al.).

**arXiv:2212.12513

*Journal of Low Temperature Physics volume 100, pages 69–104 (1995)
*Rev Sci Instrum 66, 5322–5326 (1995)

DM detectors with superconducting thermometers

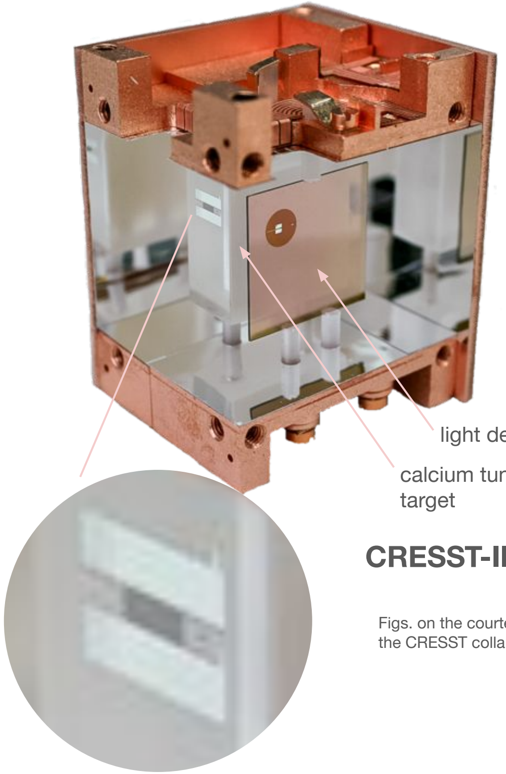

light detector

calcium tungstate target

CRESST-III DetA

Figs. on the courtesy of
the CRESST collaboration

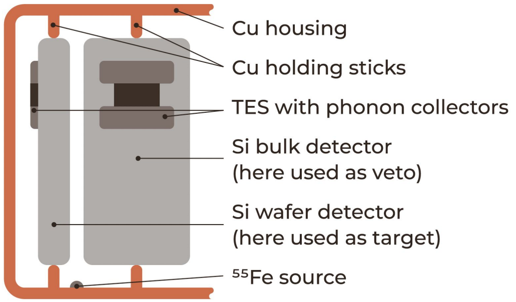

Fig. used in arXiv:2212.12513

CRESST-III Si

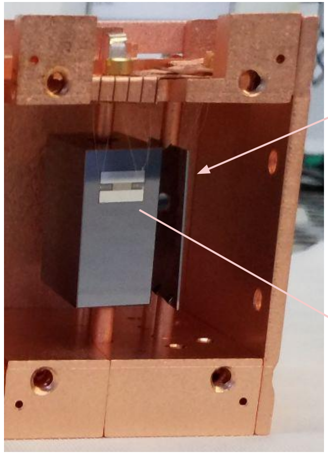

silicon wafer target

TES on main crystal

SuperCDMS-CPD

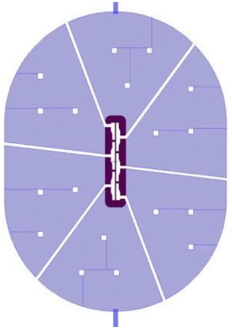

design called
“quasiparticle trap assisted
electrothermal feedback
TES” (QET)

Fig. on the courtesy of Sam Watkins
and the SuperCDMS-CPD collaboration, used in
Appl. Phys. Lett. 118, 022601 (2021)

Physics of particle recoils

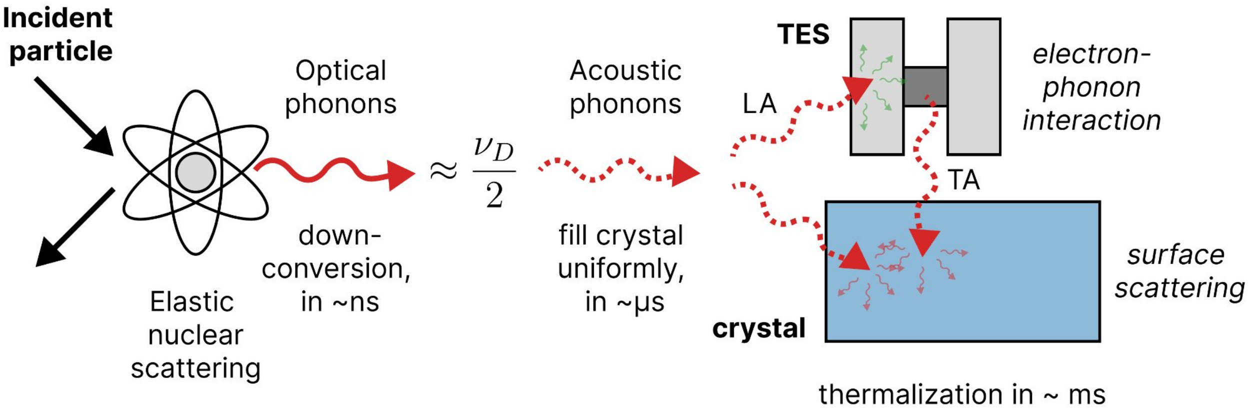

Particle recoil produces population of high energy phonons that down-convert rapidly.

Crystal is after ~µs uniformly filled, phonons thermalize within ~ms.

Share ε of athermal phonons are collected by the superconducting film and thermalize there, (1-ε) in the crystal.

Description of phonon down conversion from [Journal of Low Temperature Physics volume 100, pages 69–104 (1995)]

Electrothermal response model

System can be modeled with ordinary differential equations (ODEs), as interaction of thermal and electrical circuits:

thermal ODEs

$$C_e \frac{dT_e}{dt} + (T_e - T_a)\, G_{ea} + (T_e - T_b)\, G_{eb} = P_e(t),$$

$$C_a \frac{dT_a}{dt} + (T_a - T_e)\, G_{ea} + (T_a - T_b)\, G_{ab} = P_a(t),$$

electrical ODE

$$L \frac{dI_f}{dt} + R_s I_b - (R_f(T_e) + R_s) I_f = 0.$$

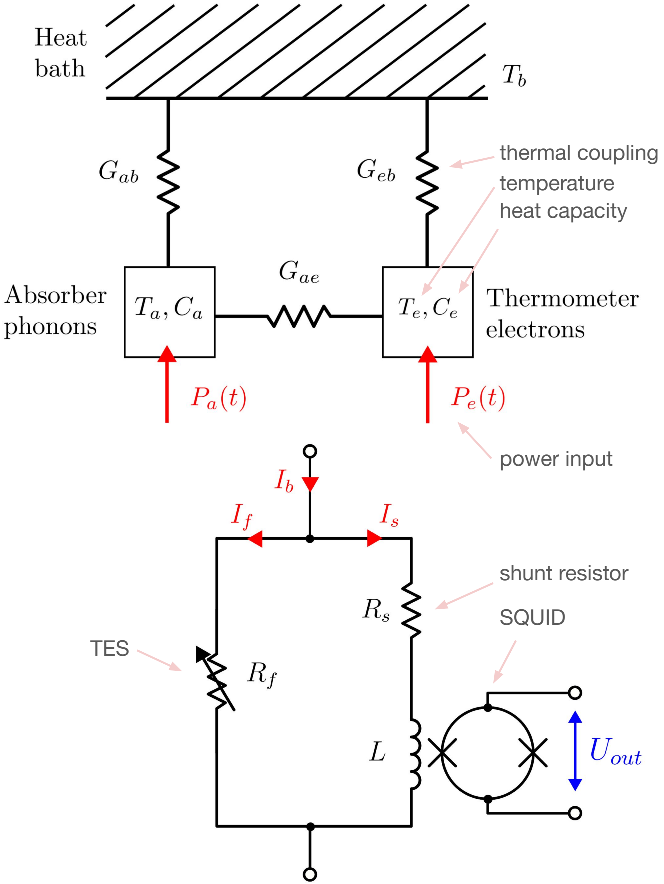

Model combined from
[Journal of Low Temperature Physics volume 100, pages 69–104 (1995)]
[Topics in Applied Physics, vol 99., Pages 63-150 (2005)]

Pulse shape

System can be simplified to describe the temperature rise from a small energy deposition ΔE ∝ ΔP:

$$\frac{d}{dt}\begin{pmatrix}\Delta T_e\\ \Delta T_a\end{pmatrix} = -\begin{pmatrix}\frac{G_{ea}+G_{eff}}{C_e} & -\frac{G_{ea}}{C_e}\\ -\frac{G_{ea}}{C_a} & \frac{G_{ea}+G_{ab}}{C_a}\end{pmatrix}\begin{pmatrix}\Delta T_e\\ \Delta T_a\end{pmatrix} + \begin{pmatrix}\frac{\Delta P_e}{C_e}\\ \frac{\Delta P_a}{C_a}\end{pmatrix}$$

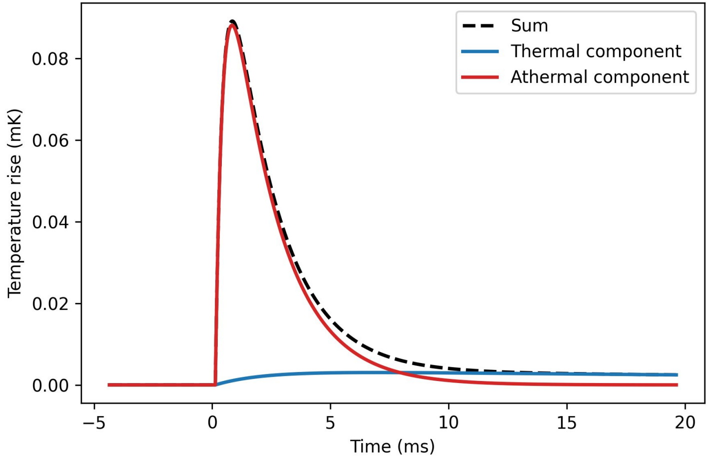

Solutions for temperature rise in thermometer are pulses of ≈ 1-100 ms length, with two components and three time constants:

crystal relaxation time

$$\Delta T_e(t) = \Theta(t)\left[A_n\left(e^{-t/\tau_n} - e^{-t/\tau_{in}}\right) + A_t\left(e^{-t/\tau_t} - e^{-t/\tau_n}\right)\right]$$

(formulas in appendix)

thermometer relaxation time

phonon thermalization time

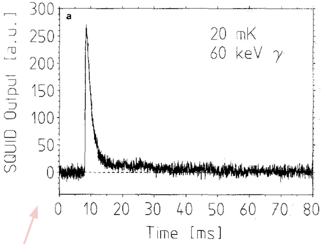

measured pulse for comparison

Model and Fig. of measured pulse from [Journal of Low Temperature Physics volume 100, pages 69–104 (1995)]

Thermal properties

Debye model (phononic system):

$$G_{ab} \propto T^3$$

$$C_{ph} = \frac{12\pi^4}{5} n_a k_B \left(\frac{T}{\Theta_D}\right)^3$$

Debye temperature

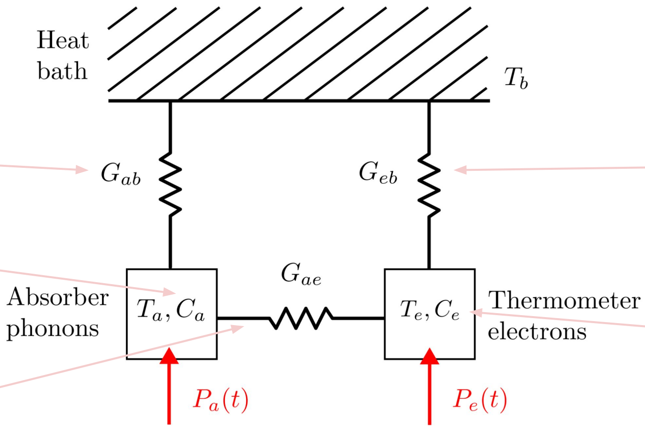

Wiedemann Franz law (electronic system):

$$G_{eb} \propto T$$

Sommerfeld model (electronic system):

$$C_e = \frac{\pi^2}{2} n_e k_B \frac{T}{T_F} = \gamma T$$

Sommerfeld constant

$$G_{ea} = \left(\frac{1}{G_{ep}} + \frac{1}{G_K}\right)^{-1}$$

$G_{ep} \propto T^5$ — electron-phonon coupling (dominating)

$G_K \propto T^3$ — Kapitza resistance

$$P_a(t) = (1-\epsilon)\frac{\Delta E}{\tau_n}\exp(\frac{t}{\tau_n}) \qquad P_e(t) = \epsilon\frac{\Delta E}{\tau_n}\exp(\frac{t}{\tau_n})$$

Effective phonon thermalization time: $\tau_n = \left(\frac{1}{\tau_{\text{film}}} + \frac{1}{\tau_{\text{crystal}}}\right)^{-1}$

Athermal phonon collection efficiency: $\epsilon = \frac{\tau_{\text{crystal}}}{\tau_{\text{crystal}} + \tau_{\text{film}}}$

Competing thermalization times in film and crystal:

$$\tau_{\text{film}} = \frac{\tau_0}{\bar{\eta}} \qquad \tau_{crystal} \propto \frac{V_a}{A_a \Theta_D}$$

Ideal film thermalization:

$$\tau_0 = \frac{2V_a}{A\langle v_\perp \alpha\rangle}$$

Mode-average phonon velocity, transmission c.:

$$\langle v_\perp \alpha\rangle \propto \Theta_D$$

Absorption coeff.:

$$\bar{\eta} \propto T$$

Volume absorber

Surface absorber

Interface TES

Model from
[Journal of Low Temperature Physics volume 100, pages 69–104 (1995)]

Optimizing athermal phonon collection

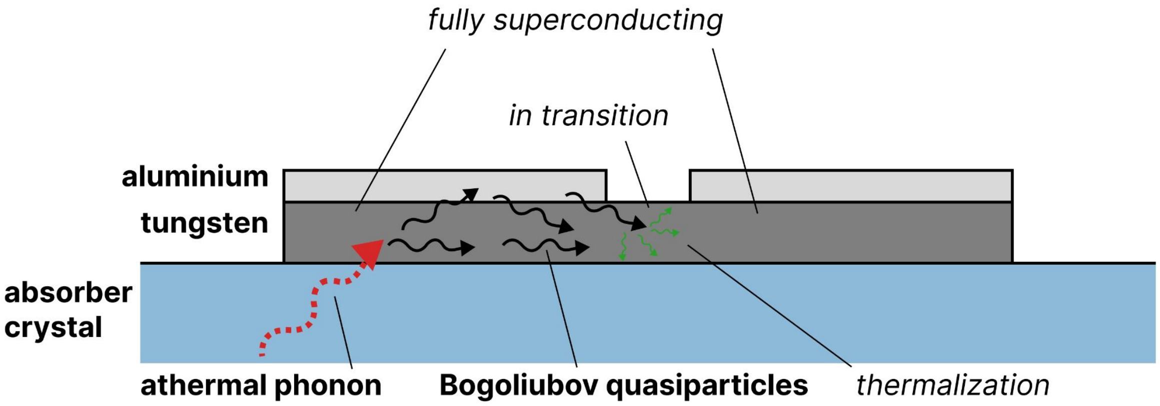

$$T \approx 15 \text{ mK} \approx T_{c,W} \ll T_{c,Al}$$

For optimized detectors, sensitivity (pulse height and area) is

$$\propto \varepsilon \Delta E / C_e$$

Collection efficiency ε can be increased without adding heat capacity, through phonon collectors.

Aluminium/tungsten bilayer is kept through proximity effect in superconducting state (exponentially suppressed heat capacity). Scattering **athermal phonons break cooper pairs** that travel diffusively to the uncovered tungsten film.

Noise model

Similarly to the pulse shape model, a model for noise contributions can be derived, depending on the occurring power and voltage fluctuations in the circuit, and the bias heating P_J:

$$C_e \frac{dT_e}{dt} + (T_e - T_b)G_{eb} = \Delta P_{e,noise} + P_J,$$

$$-L\frac{dI_f}{dt} + R_S I_b - (R_f(T_f) + R_S)I_f = \Delta U_{noise},$$

Solution of the system is a transition matrix S, which translates fundamental fluctuations to observable currents in the readout circuit I_f:

$$\begin{pmatrix} \Delta T_e \\ \Delta I_f \end{pmatrix} \stackrel{\text{def}}{=} \begin{pmatrix} s_{11}(w) & s_{12}(w) \\ s_{21}(w) & s_{22}(w) \end{pmatrix} \begin{pmatrix} \Delta P_e \\ \Delta U \end{pmatrix}$$

(formulas in appendix)

Model adapted from
[Topics in Applied Physics, vol 99., Pages 63-150 (2005)]

Fundamental sensor noise contributions

1) Electrical, Johnson noise from movement of electrons in shunt with temperature T_S and film in superconducting transition with resistance R_{f0}:

$$|\Delta U|^2_{J_s} = 4k_B T_s R_s \qquad |\Delta U|^2_{Jf} = 4k_B T_e R_{f0}$$

2) Phonon noise from thermal fluctuations between TES and heat bath:

$$|\Delta P_e|^2_{ph} = 4k_B T_e^2 G_{eb} \frac{2}{5} \frac{1-\left(\frac{T_b}{T_{e0}}\right)^5}{1-\left(\frac{T_b}{T_{e0}}\right)^2}$$

3) TES-intrinsic 1/f excess-flicker noise:

$$|\Delta P_e|^2_{flicker} = \frac{\left(\frac{\Delta R_{f,flicker}}{R_{f0}}\right)^2 R_{f0}^2}{w^\alpha} I_{f0}^2$$

4) “White” SQUID noise.

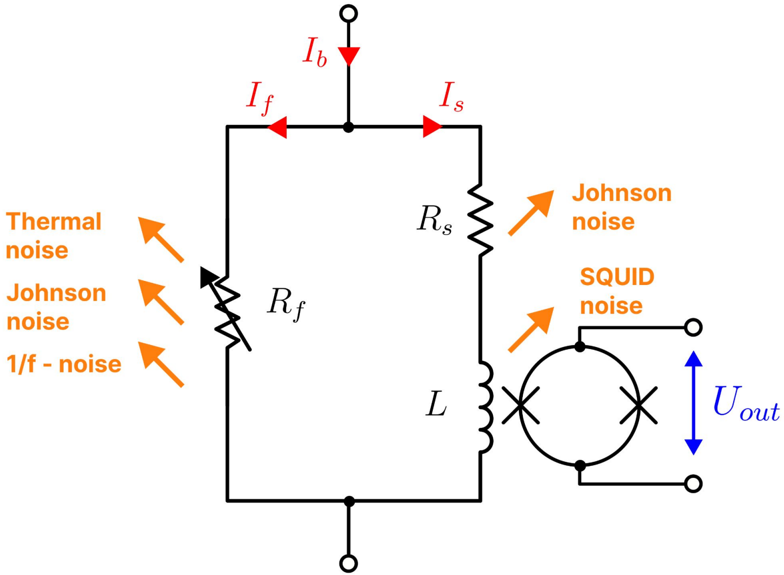

Noise description from [Topics in Applied Physics, vol 99., Pages 63-150 (2005)]

Intrinsic excess noise

Internal Thermal Fluctuation Noise (ITFN): thermometer is spacially extended object, consists therefore of a system of connected heat capacities ⇒ thermal fluctuations exist between them. Higher normal resistance can make it worse.

Excess electrical noise*: spectral shape similar to Johnson noise, larger for lower normal resistance and operation low in the transition, affected by homogeneity of film and magnetic field.

1/f-noise*: spectral shape rises steeply towards lower frequencies, cutoff << 1 Hz, often correlated with excess electrical noise.

Telegraph noise*: associated with certain bias values and points in transition curve. Possibly due to structure reordering in metallic film.

Possible sources: non-equilibrium effects, fundamental effects of superconductivity or electron-phonon interaction.

***Origin of this noise is not fully understood.**

Noise description from
[Topics in Applied Physics, vol 99., Pages 63-150 (2005)]

Exemplary detector response

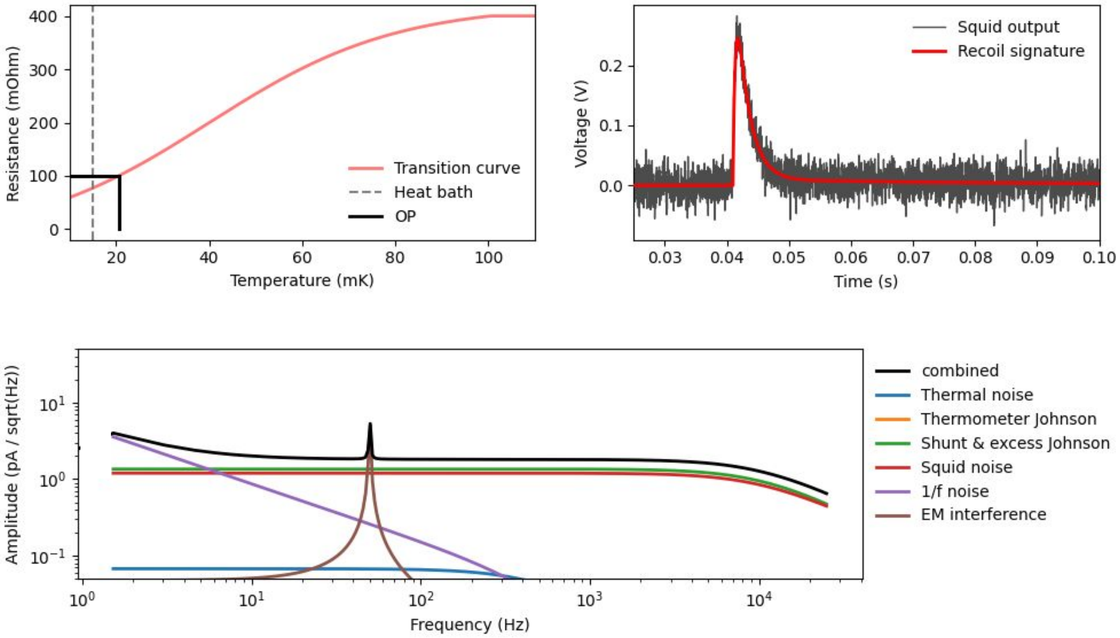

Simulation of detector with silicon target and iridium/gold bilayer TES, based on introduced response and noise models.

Transition curves of modern devices are much steeper, with a width of ≈ 1-2 mK.

Detector simulated with reference thermal properties from
[Journal of Low Temperature Physics volume 100, pages 69–104 (1995)]
Assuming fixed geometry.

Optimizing thermal couplings

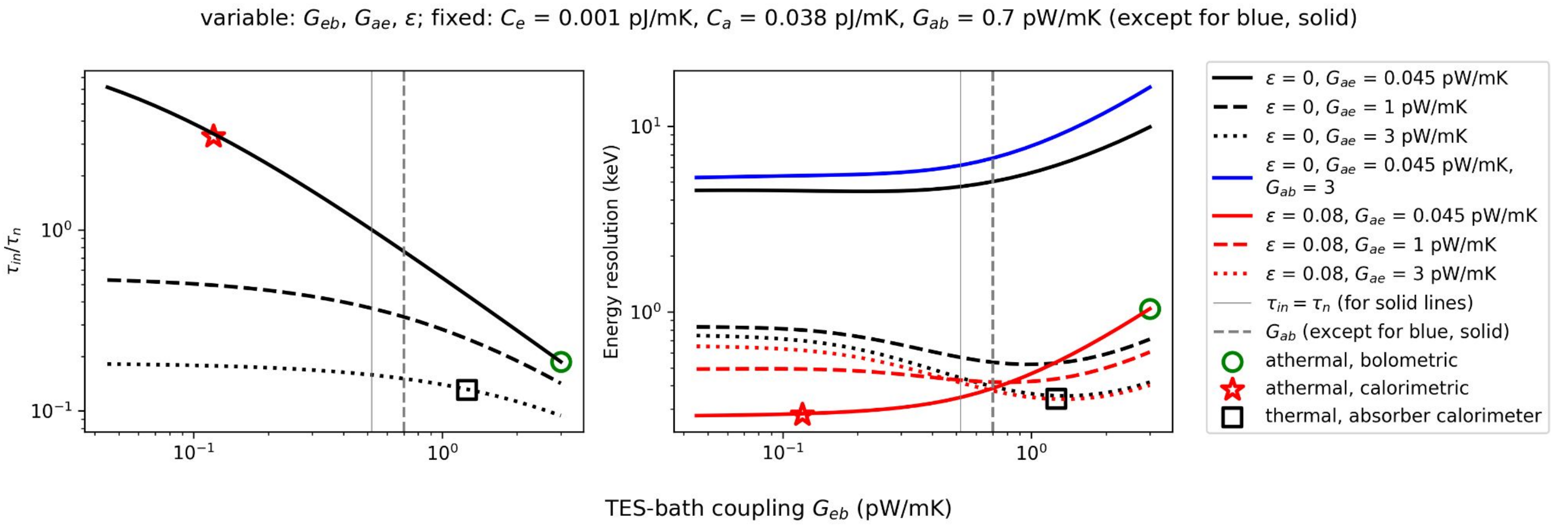

Ratio of thermometer relaxation time τ_{in} to phonon thermalization time τ_n separates **bolometric** (measuring power) and **calorimetric** (measuring energy) modi.

Most modern devices are **athermal calorimeters**.

Small, thermal detectors can reach comparable thresholds, but scale differently.

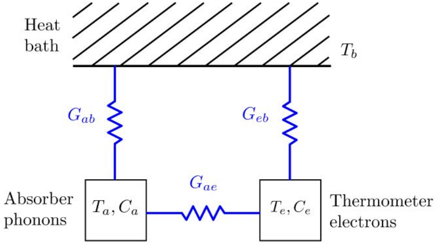

Detector simulated with reference thermal properties from
[Journal of Low Temperature Physics volume 100, pages 69–104 (1995)]
Assuming fixed geometry.

Scaling absorber volume

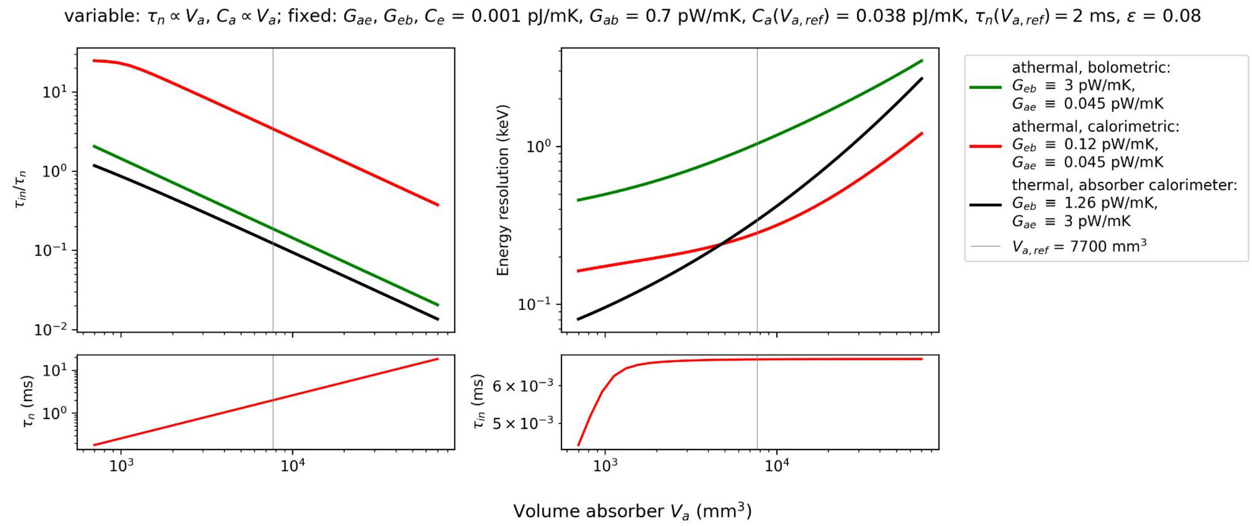

Threshold of **thermal** detector scales **∝ V_a**,

athermal detector scales **∝ $V_a^{2/3}$**.

⇒ Operating large target with low threshold challenging,

lower threshold achievable by consequently **lowering target mass**!

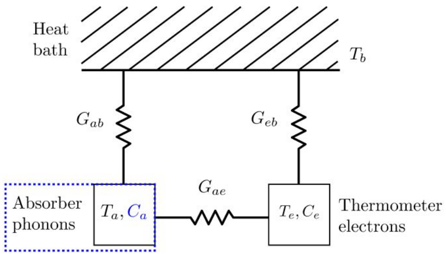

Detector simulated with reference thermal properties from
Journal of Low Temperature Physics volume 100, pages 69–104 (1995)
Assuming fixed geometry.

Scaling operation temperature

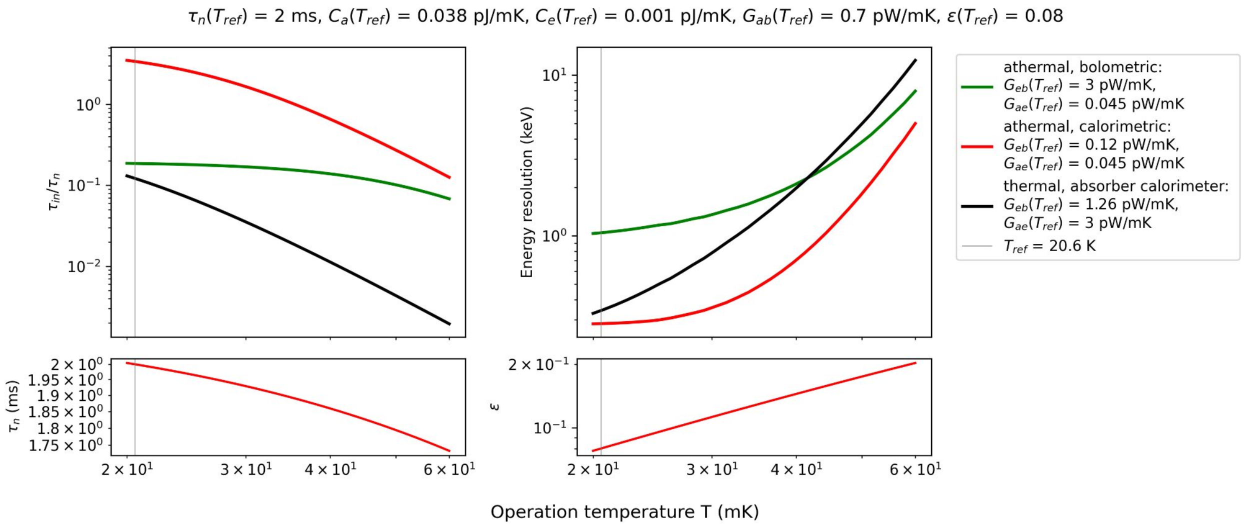

Thermal couplings scale strongly with temperature: $G_{ae} \propto T^5$.

Calorimetric modus only possible **at lowest ≈10-30 mK temperatures**!

Heat capacities decrease with temperature ⇒ sensitivity improves.

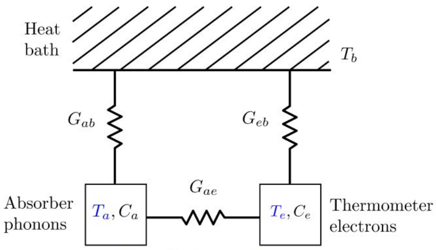

*also affects couplings, capacities, ...

Detector simulated with reference thermal properties from
Journal of Low Temperature Physics volume 100, pages 69–104 (1995)
Assuming fixed geometry.

Low energy excess events

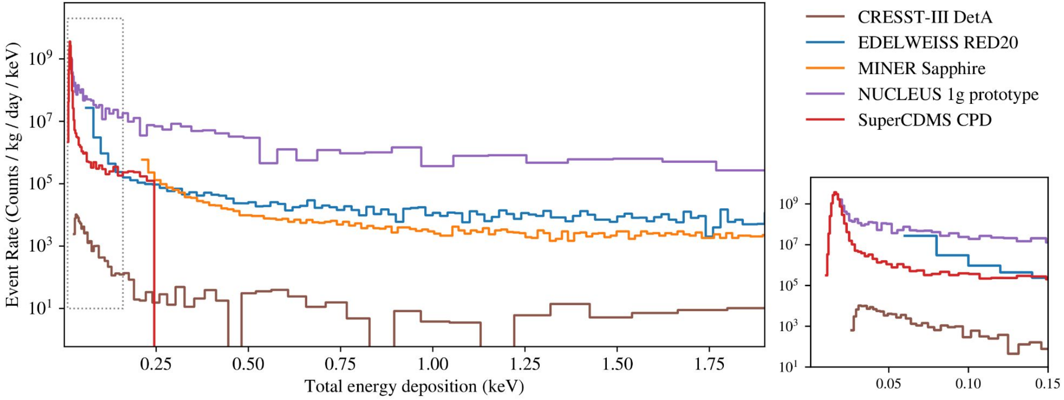

Fig. from EXCESS workshop summary SciPost Phys. Proc. 9, 001 (2022)

Experiments observe steeply rising non-ionising background towards lower energies ≈<100 eV. Event rate …

- … apparently uncorrelated with detector mass, surface, surroundings and temperature.
- … decays after cool down of experiment, on time scale of O(months)*.

Currently most probable hypothesis: **stress effect**, e.g. on crystal-thermometer interface.

Ongoing community-organized workshop series to discuss the excesses: EXCESS workshop.

*arXiv:2207.09375
*Nature Physics volume 18, pages 145–148 (2022)

Relations to other quantum technologies

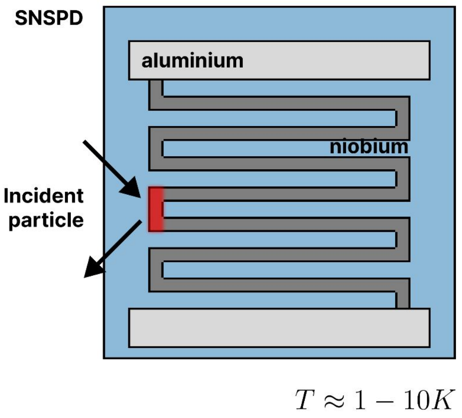

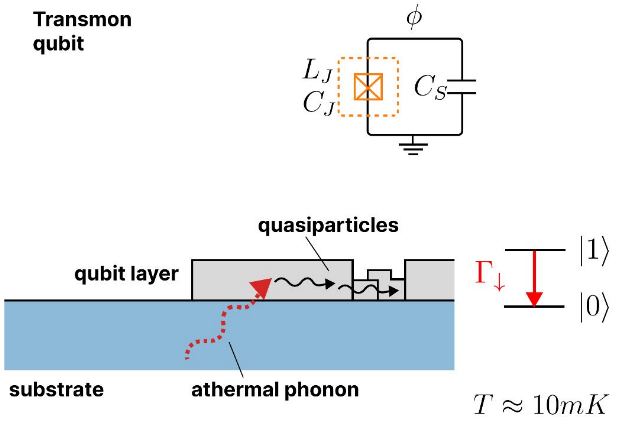

Superconducting nanowire single-photon detector (SNSPD):

- Wire is operated slightly below T_c.
- Difference to TES: sensor is target.
- Recoil needs to warm wire only locally for measurable effect.
- Can reach lower energy resolution.
- Cannot collect significant exposure.

Radiation and quasiparticle poisoning are harmful error source for superconducting qubits.

Phonon population in substrate, induced by radiation or possibly the low energy excess, can break cooper pairs in qubit layer.

Similar effect as in phonon collectors of TES.

Fig. adapted from
Nature Physics volume 18, pages 107–111 (2022)

Qubit errors through radiation discussed in
Nature volume 594, pages 369–373 (2021)
Nature Communications volume 12, Article number: 2733 (2021)
Nature Physics volume 18, pages 107–111 (2022)
The European Physical Journal C volume 83, Article number: 94 (2023)

Qubit errors through quasiparticle excess discussed in
Nature Physics volume 18, pages 145–148 (2022)
arXiv:2208.02790

Summary

- Cryogenic detectors with superconducting thermometers are currently the **most sensitive devices for sub-GeV/C^2 DM searches**.
- Lowest achieved nuclear recoil energy threshold is **10 eV.**
- Sensitivity in calorimetric mode is dominated by capability to **collect athermal phonons** from target.
- Similar challenges in fabrication and background mitigation with other superconducting technologies: SNSPDs, transmon qubits, ...
- Devices are continuously improved, new phenomena continue to be discovered and research is done to understand them: **low energy excess** events and excess noise.

Special thanks for inputs and discussions in preparation of this lecture to many members of the CRESST and COSINUS collaborations!

Appendices

Formulas for pulse shape model

$$= -I_f^2 \frac{(R_{f0} - R_s)}{(R_{f0} + R_s)} \left. \frac{dR_f}{dT_e} \right|_{T_{e0}} \qquad G_{eff} = G_{eb} + G_{ETF}$$

$$\stackrel{\text{def}}{=} -G_{ETF}.$$

$$\lambda_{1,2} = \frac{-a \mp \sqrt{a^2 - 4b}}{2} \stackrel{\text{def}}{=} -\frac{1}{\tau_{1,2}} \qquad \left(\stackrel{\text{def}}{=} -\frac{1}{\tau_{in,t}} \stackrel{\text{def}}{=} -s_{in,t} \right),$$

with

$$a \stackrel{\text{def}}{=} \frac{(G_{ea} + G_{eff})C_a + (G_{ea} + G_{ab})C_e}{C_e C_a}, \qquad b \stackrel{\text{def}}{=} \frac{(G_{ea} + G_{eff})(G_{ea} + G_{ab}) - G_{ea}^2}{C_e C_a}.$$

$$\alpha_{1,2} \stackrel{\text{def}}{=} 1 + \frac{G_{ab}}{G_{ea}} + \lambda_{1,2} \frac{C_a}{G_{ea}}.$$

$$A_n \stackrel{\text{def}}{=} \frac{\frac{\Delta E}{\tau_n}}{\left(1 - \frac{\alpha_2}{\alpha_1}\right)} \left(\alpha_2 \frac{(1 - \epsilon)}{C_a} - \frac{\epsilon}{C_e} \right) \left(\frac{1}{\tau_n} - \frac{1}{\tau_1} \right)^{-1}$$

$$= -\frac{P_0(s_{in} - (G_{ab}/C_a))}{\varepsilon(s_{in} - s_t)(s_{in} - s_n)} \left(\frac{s_t - (G_{ab}/C_a)}{G_{eff} - (C_e/C_a)G_{ab}} - \frac{\varepsilon}{C_e} \right)$$

$$A_t \stackrel{\text{def}}{=} -\frac{\frac{\Delta E}{\tau_n}}{\left(1 - \frac{\alpha_1}{\alpha_2}\right)} \left(\alpha_1 \frac{(1 - \epsilon)}{C_a} - \frac{\epsilon}{C_e} \right) \left(\frac{1}{\tau_n} - \frac{1}{\tau_2} \right)^{-1}$$

$$= \frac{P_0(s_t - (G_{ab}/C_a))}{\varepsilon(s_t - s_{in})(s_t - s_n)} \left(\frac{s_{in} - (G_{ab}/C_a)}{G_{eff} - (C_e/C_a)G_{ab}} - \frac{\varepsilon}{C_e} \right)$$

Model from
[Journal of Low Temperature Physics volume 100, pages 69–104 (1995)]

Definitions for noise matrix elements

$$\tau \stackrel{\text{def}}{=} \frac{C_e}{G_{eb}},$$

$$\tau_I \stackrel{\text{def}}{=} \frac{\tau}{(1-\mathcal{L}_I)},$$

$$\tau_{el} \stackrel{\text{def}}{=} \frac{L}{R_{f0}+R_S},$$

thermometer resistance
in operation point

$$\mathcal{L}_I \stackrel{\text{def}}{=} \frac{I_{f0}^2}{G_{eb}} \frac{dR_f}{dT_e}\bigg|_{T_{e0}},$$

current through
thermometer
in operation point

base temperature of
thermometer
in operation point

Model adapted from
[Topics in Applied Physics, vol 99., Pages 63-150 (2005)]

Formulas for intrinsic noise matrix elements

$$s_{21}^{int}(w) = \frac{-\frac{G_{eb}\mathcal{L}_I}{I_{f0}}}{\left(\frac{1}{(\tau)_{int}} + 2\pi wi\right) C_e \left(\frac{1}{\tau_{el}} + 2\pi wi\right) L - \frac{G_{eb}\mathcal{L}_I}{I_{f0}} (I_{f0}R_s - I_{f0}R_{f0})_{int}}$$

$$= -\frac{1}{I_{f0}} \left[\frac{L\tau}{(\tau)_{int}\tau_{el}\mathcal{L}_I} - \frac{(I_{f0}R_s - I_{f0}R_{f0})_{int}}{I_{f0}} \right.$$

$$\left. + 2\pi wi \frac{L\tau}{\mathcal{L}_I} \left(\frac{1}{(\tau)_{int}} + \frac{1}{\tau_{el}} \right) - \frac{4\pi^2 w^2 \tau L}{\mathcal{L}_I} \right]^{-1},$$

$$s_{22}^{int}(w) = \frac{\left(\frac{1}{(\tau)_{int}} + 2\pi wi\right) C_e}{\left(\frac{1}{(\tau)_{int}} + 2\pi wi\right) C_e \left(\frac{1}{\tau_{el}} + 2\pi wi\right) L - \frac{G_{eb}\mathcal{L}_I}{I_{f0}} (I_{f0}R_s - I_{f0}R_{f0})_{int}}$$

$$= -s_{21}^{int}(w) I_{f0} \frac{1}{\mathcal{L}_{\mathrm{I}}} (1 + 2\pi wi\tau).$$

Model adapted from
[Topics in Applied Physics, vol 99., Pages 63-150 (2005)]

Formulas for external noise matrix elements

$$s_{21}^{ext}(w) = \frac{-\frac{G_{eb}\mathcal{L}_I}{I_{f0}}}{\left(\frac{1}{(\tau_I)_{ext}} + 2\pi wi\right) C_e \left(\frac{1}{\tau_{el}} + 2\pi wi\right) L - \frac{G_{eb}\mathcal{L}_I}{I_{f0}}(-2R_{f0}I_{f0})_{ext}}$$

$$= -\frac{1}{I_{f0}}\left[\frac{L\tau}{(\tau_I)_{ext}\tau_{el}\mathcal{L}_I} - \frac{(-2R_{f0}I_{f0})_{ext}}{I_{f0}}\right.$$

$$\left. + 2\pi wi\frac{L\tau}{\mathcal{L}_I}\left(\frac{1}{(\tau_I)_{ext}} + \frac{1}{\tau_{el}}\right) - \frac{4\pi^2 w^2 \tau L}{\mathcal{L}_I}\right]^{-1},$$

$$s_{22}^{ext}(w) = \frac{\left(\frac{1}{(\tau_I)_{ext}} + 2\pi wi\right) C_e}{\left(\frac{1}{(\tau_I)_{ext}} + 2\pi wi\right) C_e \left(\frac{1}{\tau_{el}} + 2\pi wi\right) L - \frac{G_{eb}\mathcal{L}_I}{I_{f0}}(-2R_{f0}I_{f0})_{ext}}$$

$$= s_{21}^{ext}(w) I_{f0} \frac{\mathcal{L}_\mathrm{I} - 1}{\mathcal{L}_\mathrm{I}}(1 + 2\pi wi\tau_I).$$

Model adapted from
Topics in Applied Physics, vol 99., Pages 63-150 (2005)

Optimizing thermometer area

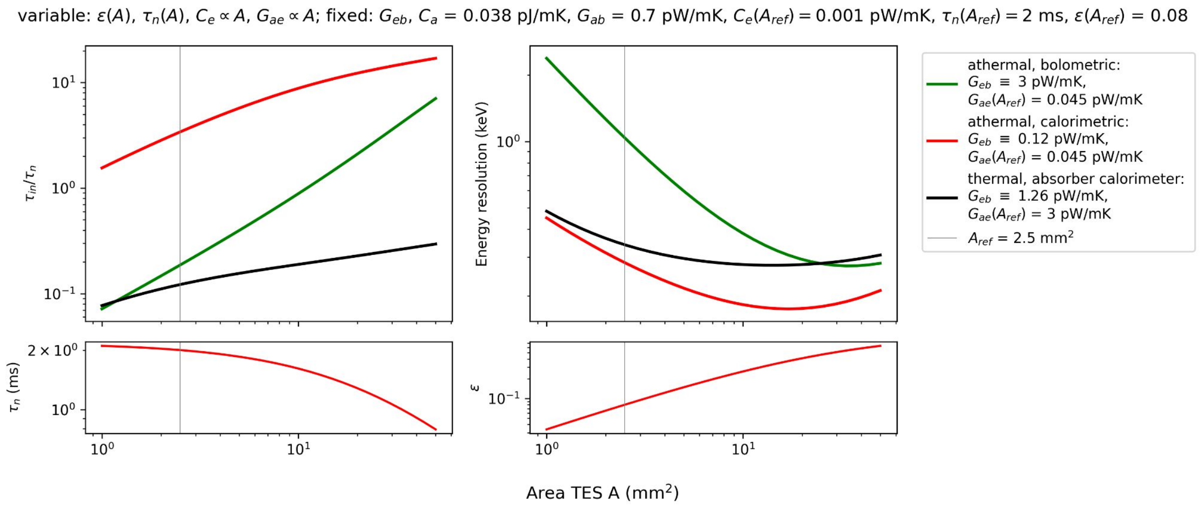

Larger thermometer increases TES heat capacity linearly, collection efficiency (slightly) nonlinearly, and TES relaxation time (almost) linearly,

⇒ for a given detector, **a broad optimum** for it's TES size exists!

Detector simulated with reference thermal properties from
[Journal of Low Temperature Physics volume 100, pages 69–104 (1995)]

Optimizing transition curves

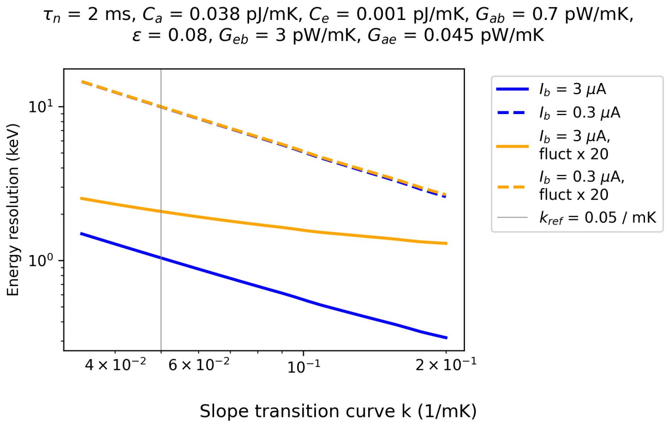

Steeper transition curve improves signal from TES resistance changes against electrical sensor noise.

⇒ **the steeper, the better** (with some practical stability constraints …)

However, if TES-intrinsic noise dominates over electrical noise, a steeper curve cannot improve the sensitivity further.

Detector simulated with reference thermal properties from
[Journal of Low Temperature Physics volume 100, pages 69–104 (1995)]